Wide bandwidth, low loss 1 by 4 wavelength division multiplexer on silicon for optical interconnects

D. T. H. Tan,[1,*] K. Ikeda,[1] S. Zamek,[1] A. Mizrahi,[1] M. P. Nezhad,[1] A. V. Krishnamoorthy,[2] K. Raj,[2] J. E. Cunningham,[2] X. Zheng,[2] I. Shubin,[2] Y. Luo,[2] and Y. Fainman[1]

[1]Dept. of Electrical and Computer Engineering, University of California San Diego, 9500 Gilman Dr. La Jolla, California 92093-0407, USA
[2]Oracle, 9515 Town Centre Drive, San Diego, California 92121, USA
**thtan@ucsd.edu*

Abstract: We demonstrate an add/drop filter based on coupled vertical gratings on silicon. Tailoring of the channel bandwidth and wavelength is experimentally demonstrated. The concept is extended to implement a 1 by 4 wavelength division multiplexer with 6nm channel separation, 3nm bandwidth, a flat top response with < 0.8dB ripple within the 3dB passband, 1dB insertion loss and 16dB crosstalk suppression. The device is ultracompact, having a footprint < 2 X 10^{-9}m^2.

OCIS codes: (130.7408) Wavelength filtering devices; (130.3120) Integrated optics devices; (130.2790) Guided waves.

References and links

1. A. V. Krishnamoorthy, R. Ho, X. Zheng, H. Schwetman, J. Lexau, P. Koka, G. Li, I. Shubin, and J. E. Cunningham, "Computing microsystems based on silicon photonic interconnects," Proc. IEEE **97**, 1337–1361 (2009).
2. G. T. Reed, G. Mashanovich, F. Y. Gardes, and D. J. Thomson, "Silicon optical modulators," Nat. Photonics **4**(8), 518–526 (2010).
3. A. Liu, R. Jones, L. Liao, D. Samara-Rubio, D. Rubin, O. Cohen, R. Nicolaescu, and M. Paniccia, "A high-speed silicon optical modulator based on a metal-oxide-semiconductor capacitor," Nature **427**(6975), 615–618 (2004).
4. Q. Xu, B. Schmidt, J. Shakya, and M. Lipson, "Cascaded silicon micro-ring modulators for WDM optical interconnection," Opt. Express **14**(20), 9431–9435 (2006).
5. O. I. Dosunmu, D. D. Can, M. K. Emsley, L. C. Kimerling, and M. S. Unlu, "High-speed resonant cavity enhanced Ge photodetectors on reflecting Si substrates for 1550-nm operation," IEEE Photon. Technol. Lett. **17**(1), 175–177 (2005).
6. T. Pinguet, B. Analui, E. Balmater, D. Guckenberger, M. Harrison, R. Koumans, D. Kucharski, Y. Liang, G. Masini, A. Mekis, S. Mirsaidi, A. Narasimha, M. Peterson, D. Rines, V. Sadagopan, S. Sahni, T. J. Sleboda, D. Song, Y. Wang, B. Welch, J. Witzens, J. Yao, S. Abdalla, S. Gloeckner, and P. De Dobbelaere, "Monolithically integrated high-speed CMOS photonic transceivers," Proc. IEEE conference on Group IV Photonics, 362–364 (2008).
7. H. Park, A. W. Fang, R. Jones, O. Cohen, O. Raday, M. N. Sysak, M. J. Paniccia, and J. E. Bowers, "A hybrid AlGaInAs-silicon evanescent waveguide photodetector," Opt. Express **15**(10), 6044–6052 (2007).
8. P. D. Trinh, S. Yegnanarayanan, F. Coppinger, and B. Jalali, "Silicon-on-insulator (SOI) phased-array wavelength multi-demultiplexer with extremely low polarization sensitivity," IEEE Photon. Technol. Lett. **9**(7), 940–943 (1997).
9. F. Xia, M. Rooks, L. Sekaric, and Y. Vlasov, "Ultra-compact high order ring resonator filters using submicron silicon photonic wires for on-chip optical interconnects," Opt. Express **15**(19), 11934–11941 (2007).
10. J. E. Cunningham, I. Shubin, X. Zheng, T. Pinguet, A. Mekis, Y. Luo, H. Thacker, G. Li, J. Yao, K. Raj, and A. V. Krishnamoorthy, "Highly-efficient thermally-tuned resonant optical filters," Opt. Express **18**(18), 19055–19063 (2010).
11. K. Ikeda, M. Nezhad, and Y. Fainman, "Wavelength selective coupler with vertical gratings on silicon chip," Appl. Phys. Lett. **92**(20), 201111 (2008).
12. H. C. Kim, K. Ikeda, and Y. Fainman, "Tunable transmission resonant filter and modulator with vertical gratings," J. Lightwave Technol. **25**(5), 1147–1151 (2007).
13. J. Hastings, M. Lim, J. Goodberlet, and H. I. Smith, "Optical waveguides with apodized sidewall gratings via spatial-phase-locked electron-beam lithography," J. Vac. Sci. Technol. B **20**(6), 2753 (2002).

#139010 - $15.00 USD Received 1 Dec 2010; revised 15 Jan 2011; accepted 16 Jan 2011; published 25 Jan 2011

14. D. T. H. Tan, K. Ikeda, and Y. Fainman, "Coupled chirped vertical gratings for on chip group velocity dispersion engineering," Appl. Phys. Lett. **95**(14), 141109 (2009).
15. D. T. H. Tan, K. Ikeda, R. E. Saperstein, B. Slutsky, and Y. Fainman, "Chip-scale dispersion engineering using chirped vertical gratings," Opt. Lett. **33**(24), 3013–3015 (2008).
16. D. T. H. Tan, P. C. Sun, and Y. Fainman, "Monolithic nonlinear pulse compressor on a silicon chip," Nat Commun **1**(8), 116 (2010).
17. A. Yariv, and P. Yeh, *Optical Waves in Crystals: Propagation and Control of Laser Radiation*, (Wiley, New York, 2002).
18. P. Yeh, and H. F. Taylor, "Contradirectional frequency-selective couplers for guided-wave optics," Appl. Opt. **19**(16), 2848–2855 (1980).
19. A. C. Turner, C. Manolatou, B. S. Schmidt, M. Lipson, M. A. Foster, J. E. Sharping, and A. L. Gaeta, "Tailored anomalous group-velocity dispersion in silicon channel waveguides," Opt. Express **14**(10), 4357–4362 (2006).
20. D. T. H. Tan, K. Ikeda, and Y. Fainman, "Cladding-modulated Bragg gratings in silicon waveguides," Opt. Lett. **34**(9), 1357–1359 (2009).
21. P. Dumon, I. Christiaens, W. Bogaerts, V. Wiaux, J. Wouters, S. Beckx, D. Van Thourhout and R. Baets, "Microring resonators in Silicon-on-insulator," in Proc. European Conf. on Integrated Optics, 196–199 (2005).
22. A. M. Prabhu, A. Tsay, Z. Han, and V. Van, "Extreme Miniaturization of Silicon Add–Drop Microring Filters for VLSI Photonics Applications," IEEE Photon. J. **2**, 436–444 (2010).
23. T. Fukazawa, F. Ohno, and T. Baba, "Very compact arrayed-waveguide-grating demultiplexer using Si photonic wire waveguides," Jpn. J. Appl. Phys. **43**(No. 5B), L673–L675 (2004).
24. T. Pinguet, B. Analui, E. Balmater, D. Guckenberger, M. Harrison, R. Koumans, D. Kucharski, Y. Liang, G. Masini, A. Mekis, S. Mirsaidi, A. Narasimha, M. Peterson, D. Rines, V. Sadagopan, S. Sahni, T. J. Sleboda, D. Song, Y. Wang, B. Welch, J. Witzens, J. Yao, S. Abdalla, S. Gloeckner, and P. De Dobbelaere, "Monolithically Integrated High-Speed CMOS Photonic Transceivers," in Proc. IEEE conference on Group IV Photonics, 362–364, (2008).

1. Introduction

Future advances in computer speeds are contingent on augmenting intra- and inter-chip bandwidth. Increases in power efficiency per bit of data is projected to be achieved by replacing electrical interconnects with their optical counterparts in the near future [1]. The implementation of photonic circuits for the purpose of chip-level communications requires devices such as modulators [2–4], detectors [5–7] and wavelength division multiplexers (WDM) [8–10]. In order to leverage the mature semiconductor fabrication infrastructure, implementation of optical interconnects on the ubiquitous silicon on insulator (SOI) platform is necessary. To date, most WDM developed for optical interconnects are based on ring resonator technology [9,10]. However, the drawback of ring resonators is their support of multiple resonant modes, giving rise to a limited free spectral range (FSR) of ~20nm. In the context of optical interconnects, this drawback implies that only a limited bandwidth may be utilized for transmission of data bits. In this paper, we demonstrate a highly compact, 1 by 4 wavelength division multiplexer (WDM) without the aforementioned limitations in bandwidth allocation. The achieved WDM has a flat channel response of < 0.8dB ripple, low insertion loss of 1dB and crosstalk suppression of 16dB. In addition, the large 3dB channel bandwidth of 3nm circumvents the need for active thermal tuning for wavelength stabilization, thus ensuring low power operation of the WDM. The demonstrated WDM is based on cascaded add/drop filters implemented using coupled vertical gratings. Tailoring of the bandwidth and operation wavelength of the constituent add/drop filters is also demonstrated.

2. Fabrication and characterization of coupled vertical grating add/drop filter

The add/drop filter forming the basis of the 1 by 4 WDM is based on coupled vertical gratings [11–16]. The schematic of the add/drop filter and a typical fabricated device are shown in Fig. 1(a) and 1(b) respectively. The add/drop filter is fully reciprocal, and is composed of two waveguide gratings, WG1 and WG2 with sinusoidally corrugated sidewalls, separated by a

#139010 - $15.00 USD Received 1 Dec 2010; revised 15 Jan 2011; accepted 16 Jan 2011; published 25 Jan 2011

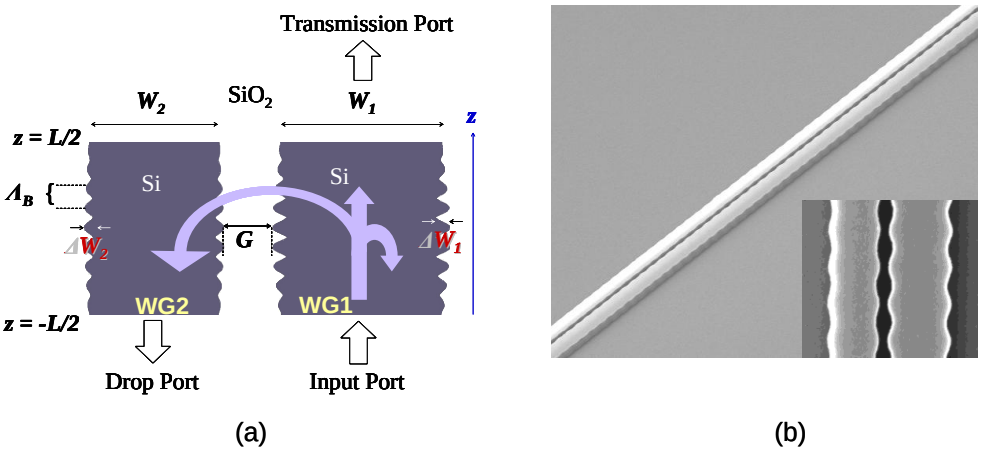

Fig. 1. (a) Schematic of coupled vertical grating add/drop filter. (b) Scanning electron micrographs of a typical fabricated add/drop filter.

gap width, G. The average waveguide widths are denoted by $W_{1,2}$ and the sidewall modulation amplitudes are denoted by $\Delta W_{1,2}$. The waveguide grating period, Λ_B is identical in both gratings. The total filter length is denoted by L. In order to reduce out of band sidelobes, a raised cosine apodization filter is applied to modulate the coupling coefficient from zero at the extreme ends of the waveguides to its maximum value at the center. Optical fields at the add/drop filter wavelength of operation are incident at the input port and Bragg coupled into the drop port [11]. Optical fields at all other wavelengths are transmitted unperturbed. The filter is implemented on a CMOS compatible SOI platform with a 250nm Si top layer on a 3μm buried oxide layer. The wavelength of operation, λ_B is governed by the equation [17,18],

$$\Lambda_B = \lambda_B / [n_{eff_1}(\lambda_B) + n_{eff_2}(\lambda_B)] \quad (1)$$

where $n_{eff1,2}$ are the effective indices of $WG_{1,2}$. Tailoring of the filter bandwidth, $\Delta\lambda$ is achieved by varying G. A smaller value of G results in a larger overlap integral of the counter-propagating fields with the sidewall corrugation, leading to a larger filter bandwidth. In addition to Bragg cross coupling leading to the add/drop filter's functionality as governed by Eq. (1), the sidewall corrugation on WG1 and WG2 lead to two additional Bragg conditions. The Bragg condition brought about by WG1 and WG2 places an upper and lower limit respectively on the free spectral range of the add/drop filter. The center wavelength, $\lambda_{FSR1,2}$ of the upper and lower limits are calculated using,

$$\lambda_{FSR1,2} = 2.n_{eff\,1,2}\left(\lambda_{FSR1,2}\right).\Lambda_B \quad (2)$$

Unlike add/drop filters implemented using ring resonators, the add/drop filter demonstrated here is not limited by its FSR, and therefore allows much more efficient bandwidth allocation within the C-band.

For demonstration of tailoring of the add/drop filter bandwidth, we utilize the following parameters. W_1 = 500nm and W_2 = 400nm, ΔW_1 = 50nm and ΔW_2 = 30nm. $n_{eff1,2}$ for these values of $W_{1,2}$ are calculated using a fully vectorial, 3D beam propagation method. The calculated propagation constants provide a more accurate measure of the Bragg wavelengths as compared to prior work [11], where the effective indices were calculated in 2D. It follows from Eq. (1) that for λ_B = 1.55μm, Λ_B = 318nm. Using Eq. (2), λ_{FSR1} is calculated to be centered at ~1.59μm and λ_{FSR2} is calculated to be centered at ~1.51μm. Increasing the FSR limits may be achieved by increasing W_1 or decreasing W_2. In increasing the value of W_1, inverse tapers can be used to ensure that only the fundamental mode is excited [19]. The stop bands brought about by the Bragg conditions within WG1 and WG2 lead to a small reduction

#139010 - $15.00 USD Received 1 Dec 2010; revised 15 Jan 2011; accepted 16 Jan 2011; published 25 Jan 2011

in the FSR. Using a cladding modulated Bragg grating implementation described in Ref. 20, weaker coupling coefficients within WG1 and WG2 may be implemented leading to smaller spectral bandwidths from self-Bragg coupling. This will enable the device FSR to be extended. Dispersion plots for $2\beta_1$, $2\beta_2$ and $\beta_1 + \beta_2$ are shown in Fig. 2, where $\beta_{1,2}$ are the propagation constants for $WG_{1,2}$. The intersection points of each of the three plots with the horizontal dotted line, $2\pi/\Lambda_B$ illustrate the three Bragg conditions leading to the FSR limits and the wavelength of operation of the add/drop filter.

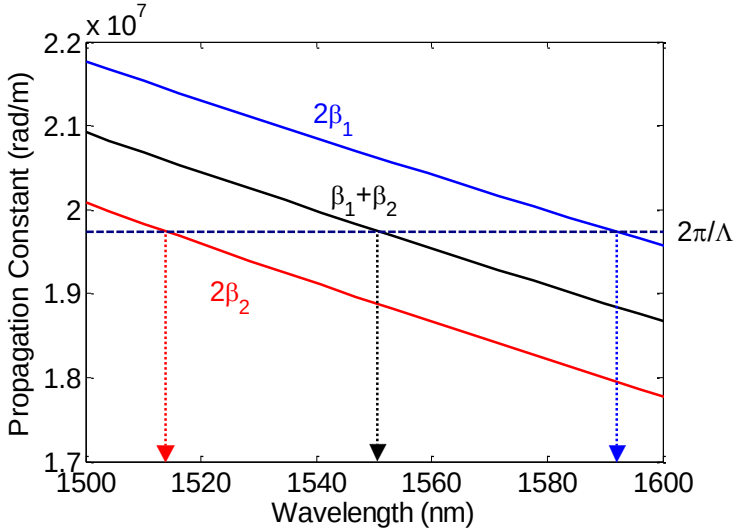

Fig. 2. Dispersion plots for $2\beta_1$, $2\beta_2$ and $\beta_1 + \beta_2$. Intersection points with $2\pi/\Lambda$ denote that the Bragg condition is satisfied, which gives rise to the add/drop filter's FSR limits and channel wavelength.

Fabrication of the add/drop filters is performed using electron beam lithography, reactive ion etching followed by plasma enhanced chemical vapor deposition of the SiO_2 overcladding. Propagation loss measured using the cutback method was 6dB/cm. Several add/drop filters with different values of G are fabricated in order to demonstrate tailoring of the filter bandwidth. All add/drop filters in this paper are terminated with inverse tapers in order to improve coupling efficiency and to minimize Fabry Perot oscillations in the measured spectra. The drop and transmission port spectra are measured using an optical spectrum analyzer with a broadband optical source adjusted for TE polarization as the input. Light from the broadband source is coupled via a tapered fiber into the add/drop filters for characterization. Figure 3(a)–3(c) shows the measured add and transmission port spectra for G = 60nm, 104nm and 160nm for L = 400μm. The stopband observed in the transmission port at ~1585nm in each of the three plots is a result of the self-Bragg coupling of WG1, and agrees well with the value of λ_{FSR1} calculated earlier. It is observed that the drop port wavelength is slightly red shifted to 1560nm. This observed shift is likely due to the fabricated value of W_2 being slightly larger than the design. The measured add/drop filter bandwidth is observed to decrease from 3nm to 1.9nm and 1.5nm as G is increased, as expected from the reduction in cross coupling strength. The reduction in coupling strength is also evident in the smaller amount of power coupled into the drop port for G = 160nm. Figure 3(d) shows a plot of the measured value of $\Delta\lambda$ as G is varied showing the inverse exponential relation between the two parameters. The asymmetric shape observed in the measured spectra is a result of imperfect tapering of the coupling coefficients from the input of the filter to the center, and again from the center of the filter to the end. By optimizing the apodization filter, further reductions in the ripples observed at higher wavelengths may be achieved, thus reducing crosstalk levels.

#139010 - $15.00 USD Received 1 Dec 2010; revised 15 Jan 2011; accepted 16 Jan 2011; published 25 Jan 2011

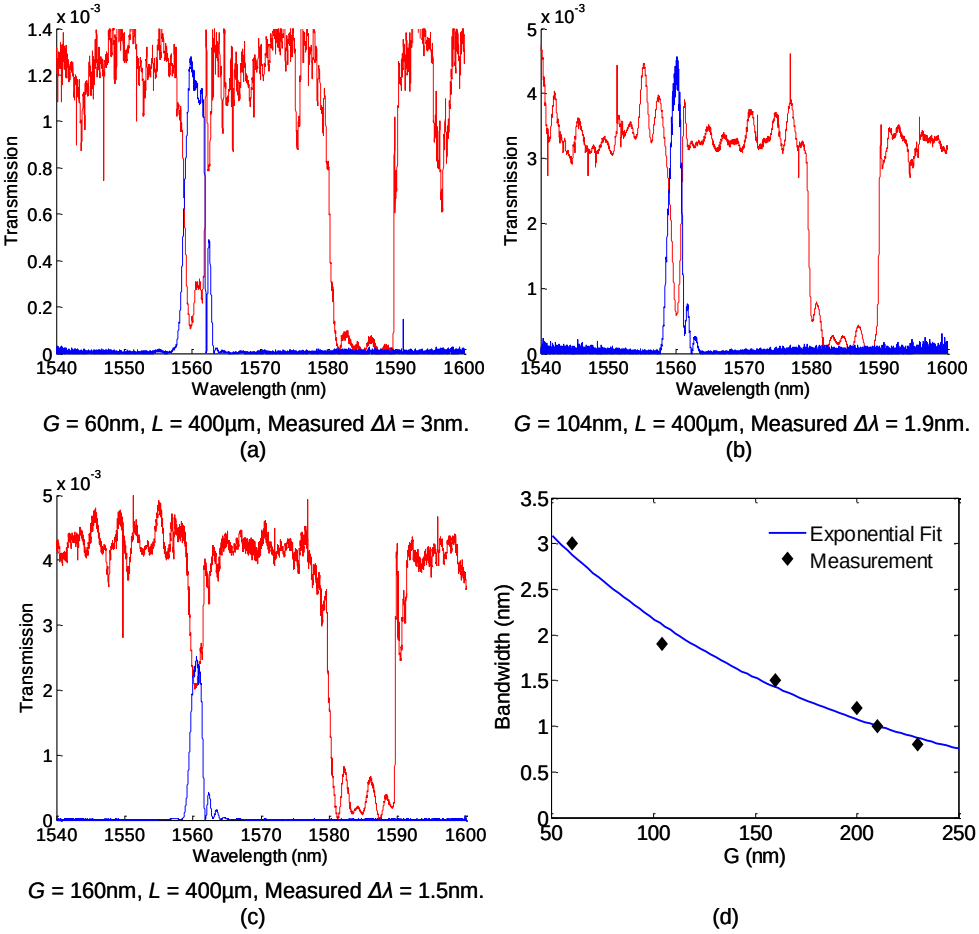

Fig. 3. (a) – (c) Measured transmission (red) and drop port (blue) spectra for fabricated add/drop filters. (d) Plot of measured $\Delta\lambda$ as a function of G showing the inverse exponential relation.

The implementation of a wavelength division multiplexer requires that the channel wavelength may be tailored such that several add/drop filters with different spectral locations may be cascaded. According to Eq. (1), tailoring the filter wavelength may be achieved by changing W_2, so as to achieve a different value of n_{eff2} and consequently, λ_B. To demonstrate the feasibility of placing additional channels, we fabricated an additional device with a slightly different value of W_2. To position the channel to the left of that demonstrated in Fig. 3(a), we require a smaller value of W_2. According to Fig. 2, a reduction in n_{eff2} by ~0.03 is necessary to shift the channel wavelength to 1.55µm. This may be achieved by decreasing W_2 by ~20nm. A device with parameters L = 400µm, and G = 60nm with W_2 20nm smaller than that of the device shown in Fig. 3(a). is fabricated. The measured drop port spectrum is plotted in Fig. 4 together with the measured spectrum shown in Fig. 3(a). The expected shift in channel wavelength from the calculated effective indices of the waveguides and the cross coupling condition is 10nm. We obtain a measured shift in the drop port by 12nm from 1.56µm to 1.548µm. Additional channels can be similarly fabricated and accurately positioned by careful design of the width, W_2.

#139010 - $15.00 USD Received 1 Dec 2010; revised 15 Jan 2011; accepted 16 Jan 2011; published 25 Jan 2011

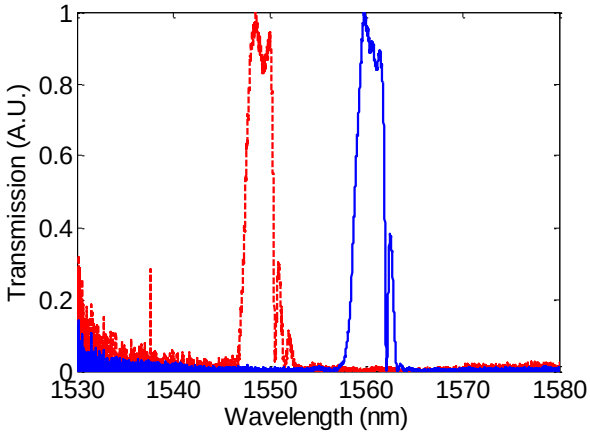

Fig. 4. Drop port measurements for G = 60nm for value of W_2 20nm smaller (red dotted line) than that of the device shown in Fig. 3(a) (blue solid line). The channel wavelength has been red shifted by 12nm because of the smaller propagation constant in WG2.

3. Design and characterization of 1 by 4 WDM

Using the add/drop filter developed in the previous section, we proceeded to implement a 1 by 4 WDM device using coupled vertical gratings. Figure 5 shows the device schematic for the 1 by 4 WDM. The device consists of a central waveguide grating, WG1 with a width, W_1 = 500nm, and sinusoidally corrugated sidewalls with a period Λ = 318nm. Four waveguide gratings with different widths, W_2, W_3, W_4, W_5, are coupled to the central waveguide in order to create 4 drop ports at different wavelengths, spaced equidistance from one another. The target features of the WDM are a low insertion loss, flat transmission response, and low inter-channel crosstalk. In addition, the WDM channel bandwidth is designed to be large in order to reduce the power required for thermal stabilization to counteract temperature fluctuations. As before, ΔW_1 is 50nm, and $\Delta W_{2,3,4,5}$ which is the sidewall modulation amplitude for each of the 4 drop ports is 30nm. The 3dB bandwidth of each of the four channels is designed to be 3nm. Channel separation is designed to be 6nm, corresponding to twice the target 3dB bandwidth. $W_{2,3,4,5}$ are adjusted to meet the target channel separation. As a result of the wavelength dependence of the optical mode and the cross coupling coefficient, a fixed gap width at shorter wavelengths will result in a decrease in the overlap integral of counter-propagating fields with the sidewall perturbation, leading to a smaller cross coupling coefficient and bandwidth. This effect is somewhat counteracted by the slight increase in modal confinement as the coupled grating width is decreased. Due to the two opposing effects, the difference is expected to be small and therefore, identical gap widths may be used to achieve a 3nm bandwidth for the four channels. The designed 1 by 4 WDM is fabricated with L = 450μm, G_2 = G_3 = G_4 = G_5 = 60nm in order to meet the target bandwidth of 3nm.

Figure 6(a) shows the measured spectra of drop ports 2 – 5 including the transmission port. The WDM spectra are normalized by the measured fiber-waveguide coupling. The demonstrated WDM has a low insertion loss of 1dB, a flat top response with < 0.8dB of ripple within the 3dB passband and 16dB inter-channel crosstalk suppression. Figure 6(b) plots an enlarged view of the measured spectrum from port 4. The flat top response will ensure that minimal amplitude distortion of data being transmitted through the channels occurs. The target design parameters of 3nm channel bandwidth and 6nm average channel separation are achieved. It is observed that the channel spacing is quite even, to an accuracy of 0.5nm. The demonstrated 1 by 4 WDM is ultracompact, having a total device footprint of (1.6μm X 950μm) < 2 X 10^{-9} m^2.

#139010 - $15.00 USD Received 1 Dec 2010; revised 15 Jan 2011; accepted 16 Jan 2011; published 25 Jan 2011

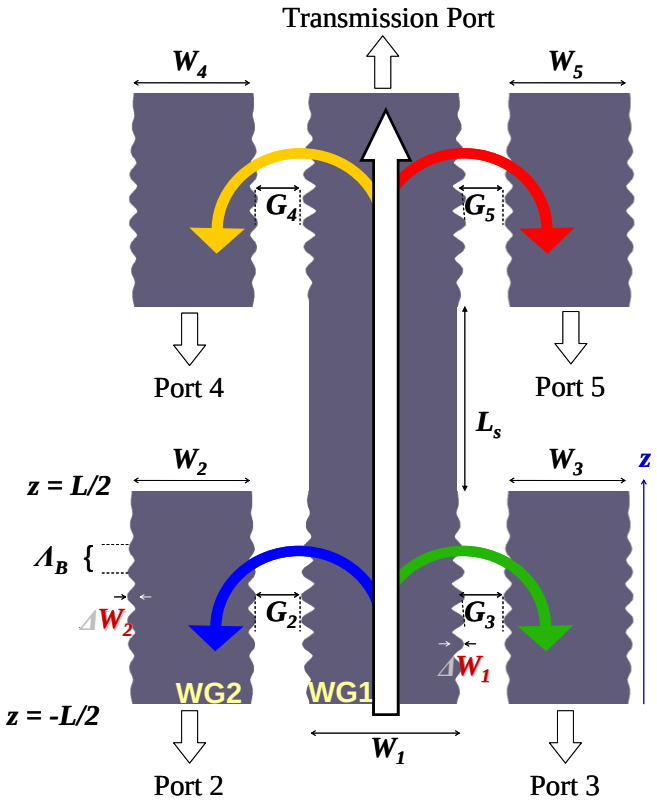

Fig. 5. (a) Schematic of 1 by 4 WDM implemented using coupled vertical grating add/drop filters. L_s = 50μm. Light incident at WG1 is cross coupled into Ports 2 – 5 at the respective Bragg wavelengths. (b) Effective index as a function of coupled grating width.

Key advantages of the WDM implemented using coupled vertical grating add/drop filters are the large free spectral range, flat response and ultra-small footprint. High order ring resonators are widely used as wavelength filtering devices. State of the art ring resonator filters featuring large 3dB bandwidths of 2-3nm have high out of band rejection ratios of up to 40dB, but have a limited FSR of ~20nm [9]. Since the FSR of ring resonators scales inversely with the radius, decreasing the ring radius may offer larger FSRs, but at the cost of larger bending and coupling losses, and poor drop efficiency [21,22]. Arrayed waveguide gratings (AWGs) may be designed to have large FSRs exceeding 90nm [23], but at the expense of a larger device footprint and inter-channel crosstalk. Our approach circumvents the limitation in the FSR, since each coupled grating add/drop filter has only one resonant wavelength. In order to further extend the useable bandwidth into the L-band, W_1 may be increased in order to red shift the self-Bragg coupling wavelength (1585nm) from WG1 and in so forth, obtain an even larger FSR. Consequently, wavelength division multiplexers with a larger number of channels may be implemented. However, the inter-channel crosstalk in our device falls short of that demonstrated in high order ring resonator filters [9]. Several approaches to improve the crosstalk may be taken. By increasing the sidewall modulation in WG1 and WG2, similar coupling coefficients and bandwidths may be obtained even with larger values of *G*. This approach will reduce some of the crosstalk induced by coupling of co-propagating modes between the two waveguides. In addition, further optimization of the apodization filter will enable reductions in sidelobe levels thus leading to an improvement in crosstalk. The inter-channel crosstalk suppression of 16dB achieved in our 1 by 4 WDM is close to the value of WDM components used in optical interconnects such as transceivers [24].

#139010 - $15.00 USD Received 1 Dec 2010; revised 15 Jan 2011; accepted 16 Jan 2011; published 25 Jan 2011

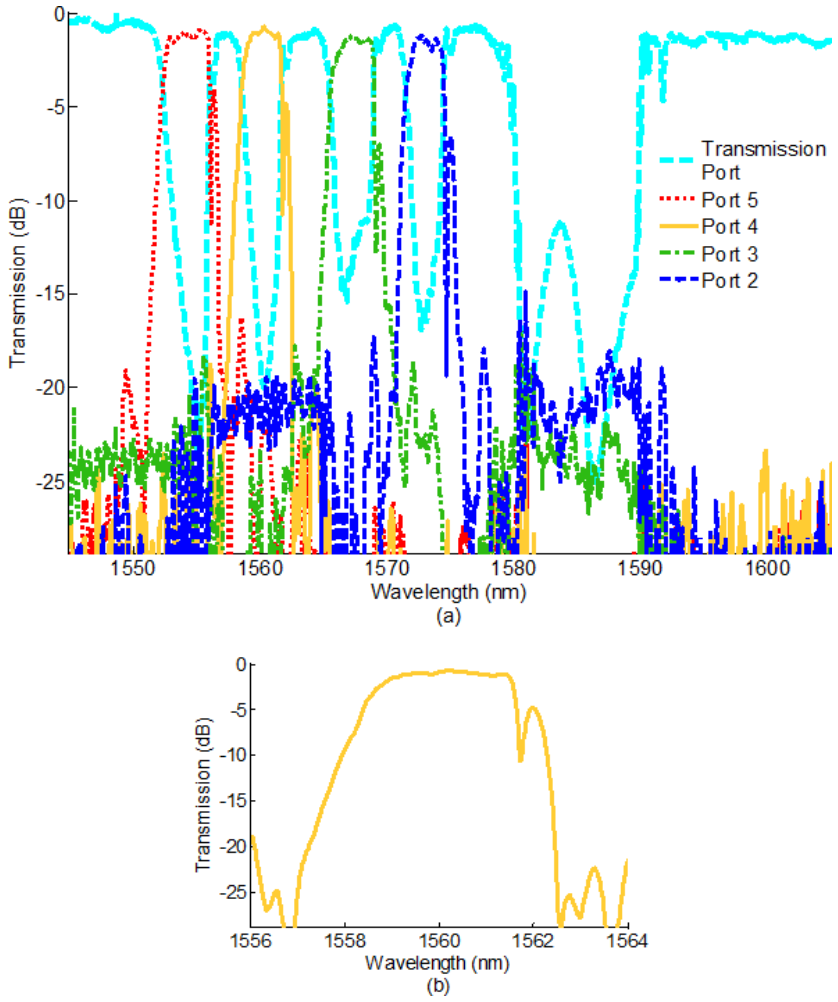

Fig. 6. (a) Measured spectral characteristics of 1 by 4 wavelength division multiplexer implemented using cascaded coupled vertical grating add/drop filters. (b) Enlarged plot of measured spectral characteristics of Port 4.

The replacement of electrical interconnects with their optical counterparts is expected to proliferate next generation's data centers and computer systems. The WDM demonstrated here is ideally suited for inter-chip level communications since it is implemented on a CMOS compatible SOI platform, with an ultra-small footprint. The large crosstalk suppression also ensures minimal crosstalk between adjacent WDM channels. Fluctuations in the operating temperature and fabrication inaccuracies can lead to shifts in the resonant wavelength. For smaller channel bandwidths, the fractional shift in wavelength can be significant. Therefore a larger bandwidth per channel has the benefit of reducing the need for active thermal tuning to ensure input data is multiplexed to the correct ports. Using the thermo-optic coefficients for silicon (1.86×10^{-4}/°C) and silicon dioxide (1.0×10^{-5}/°C), the shift in channel wavelength for port 4 as a function of temperature is calculated and shown in Fig. 7. Due to the large bandwidth, data transmitted through port 4 can withstand temperature fluctuations of ± 12°C without shifting out of the 3dB channel passband. Therefore, lower power consumption is

#139010 - $15.00 USD Received 1 Dec 2010; revised 15 Jan 2011; accepted 16 Jan 2011; published 25 Jan 2011

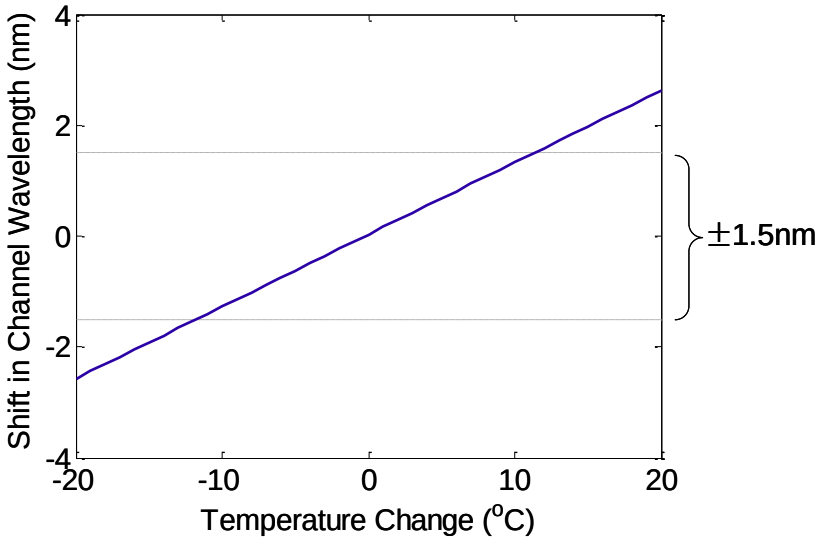

Fig. 7. Calculated shift in center wavelength for port 4 as a function of change in temperature.

required for active thermal stabilization since it is only required that the temperature is kept within this range to ensure that incoming data is routed to the correct ports without detriment. If desired however, thermal tuning of individual channel wavelengths may be performed to further counteract fabrication induced inaccuracies, and also to achieve reconfigurable add/drop multiplexers. Independent tuning of each channel may be performed thermally by placing microheaters on top of each add/drop filter [10].

4. Conclusions

We have demonstrated an add/drop filter based on coupled vertical gratings. Experimental characterization of fabricated devices shows the feasibility of tailoring channel bandwidth and wavelength. The add/drop filter concept is extended to implement a 1 by 4 WDM. Characterization of the fabricated WDM shows a 3dB bandwidth of 3nm, channel separation of 6nm, < 0.8dB ripple in the passband of each channel, an insertion loss of 1dB, and 16dB of interchannel crosstalk suppression. In addition, the device is ultracompact, having a footprint of $< 2 \times 10^{-9} m^2$. The demonstrated WDM is not FSR limited within the C-band, and may be further modified to increase its FSR to include the L-band. The large channel bandwidth reduces the energy required for active thermal tuning to reduce temperature fluctuations. The small device footprint, efficient allocation of bandwidth and potential for low power operation make the demonstrated WDM ideally suited for optical interconnects for implementation of next generation computer network architectures.

Acknowledgments

This work was supported in part by the National Science Foundation, the Defense Advanced Research Projects Agency (DARPA), the NSF CIAN ERC, the Cymer corporation, and the U.S. Army Research Office. This work was also supported in part by Oracle under contract HR0011-08-9-0001 between the government and Oracle. The views, opinions and/or findings contained in this article are those of the author/presenter and should not be interpreted as representing the official views or policies, either expressed or implied, of the Defense Advanced Research Projects Agency or the Department of Defense. Distribution Statement "A" (Approved for Public Release, Distribution Unlimited). The authors thank the UCSB nanofabrication facility for help with electron beam writing.

#139010 - $15.00 USD Received 1 Dec 2010; revised 15 Jan 2011; accepted 16 Jan 2011; published 25 Jan 2011